Biochemical and Biophysical Research Communications 597 (2022) 91–97

Contents lists available at ScienceDirect

Biochemical and Biophysical Research Communications

journal homepage: www.elsevier.com/locate/ybbrc

Effects of radiofrequency exposure on *in vitro* blood-brain barrier permeability in the presence of magnetic nanoparticles

Fatih Senturk [a, 1, *], Soner Cakmak [b], Ismail Cengiz Kocum [c], Menemse Gumusderelioglu [b], Goknur Guler Ozturk [a]

[a] Department of Biophysics, Faculty of Medicine, Gazi University, Ankara, Turkey
[b] Division of Bioengineering, Graduate School of Science and Engineering, Hacettepe University, Ankara, Turkey
[c] Department of Biomedical Engineering, Baskent University, Ankara, Turkey

ARTICLE INFO

Article history:
Received 12 January 2022
Accepted 28 January 2022
Available online 31 January 2022

Keywords:
Blood-brain barrier permeability
RF-Field
FITC-Dextran
Magnetic nanoparticles

ABSTRACT

The blood-brain barrier (BBB) remains a major obstacle for the delivery of drugs in the treatment of many neurological diseases. In this study, we aimed to investigate the effects of radiofrequency electromagnetic fields (RF-EMFs) on the permeability of an *in vitro* BBB model under RF exposure alone, or in the presence of nanoparticles (NPs). For this purpose, an *in vitro* BBB model was established by seeding human umbilical vein endothelial cells (HUVECs) and human glioblastoma cell line (T98G) on the apical and basolateral sides of the transwell membrane, respectively. The integrity of the BBB model was confirmed by measuring transendothelial electrical resistance (TEER), and a fluorescein isothiocyanate (FITC)-dextran permeability assay was performed when the resistance reached 120 Ω cm^2. After the RF-field exposure (13.56 MHz, 80 W, 10 min), we found that FITC-dextran transported across the *in vitro* BBB was increased 10-fold compared to FITC-dextran transported without an RF-field. This notable phenomenon, which can be called the burst permeability RF effect (BP-RF), has been proposed for the first time in the literature. Subsequently, the effect of the RF-field on BBB permeability was also investigated in the presence of superparamagnetic iron oxide nanoparticles (SPIONs) and magnetic poly(lactic-*co*-glycolic acid)-polyethylene glycol (PLGA-b-PEG) nanoparticles (*m*-PNPs). It was found that the amount of both transported NPs on the basolateral sides increased after exposure to the RF-field. As a result, the RF-field can be applied simultaneously during treatment with clinical agents or nanocarriers, improving the permeability of the BBB, which may contribute to therapeutic efficacy of many drugs that are used in neurological diseases.

© 2022 Elsevier Inc. All rights reserved.

1. Introduction

The blood-brain barrier (BBB) is a physical barrier that protects the central nervous system (CNS) from toxic agents, and it consists of endothelial cells surrounded by pericytes and astrocytes [1]. Unlike the other endothelial cell types, BBB endothelial cells are strongly connected by tight junctions with polarized plasma membranes [2]. Tight junctions allow nutrients and small molecules to pass through into the brain but restrict the passage of large and hydrophilic molecules [3]. Although the BBB is essential for the normal function of the central nervous system [4], it literally creates a real 'barrier' in the treatment of CNS diseases, especially tumors, by preventing various drug molecules moving through the BBB [5]. Therefore, it is critical to efficiently deliver drug molecules across the BBB to target regions to improve the outcome of the treatment modalities [6].

Blood-brain barrier permeability can be improved by using nanocarrier systems that can facilitate drug delivery to the brain due to their superior physicochemical properties [7]. Additionally, physically triggering systems (ultrasound, electromagnetic fields, etc.) hold tremendous promise for improving BBB permeability by interacting with the appropriate nanocarriers [8]. Superparamagnetic iron oxide nanoparticles (SPIONs) respond specifically to alternating magnetic fields due to their unique magnetic properties [9]. This interaction of magnetic nanocarriers and magnetic fields may increase drug transition across the BBB, thus

* Corresponding author. Department of Biophysics, Faculty of Medicine, Duzce University, Duzce, Turkey.
E-mail address: fatihsenturk@duzce.edu.tr (F. Senturk).
[1] Present address: Department of Biophysics, Faculty of Medicine, Duzce University, Duzce, Turkey.

https://doi.org/10.1016/j.bbrc.2022.01.112
0006-291X/© 2022 Elsevier Inc. All rights reserved.

contributing to therapeutic efficacy in the treatment of various CNS diseases [10]. In addition, increasing the transport ability of SPIONs across the BBB can be achieved by coating the SPIONs with biocompatible/biodegradable polymers such as poly(lactic-*co*-glycolic acid) (PLGA) and polyethylene glycol (PEG) [11].

It has been shown that electromagnetic fields can be used to increase BBB permeability in both *in vitro* and *in vivo* models [12]. Additionally, radiofrequency (RF) can modify the biophysical properties of the cell membrane, especially the electrical properties of the membrane [13]. The interaction of RF-fields with the cell membrane can alter the ionic gradient across the membrane related to ion fluxes [14]. The effectiveness of RF-fields is considered to be due to their possible nonthermal effect on the cell membrane [15]. Supporting this situation, it has been reported that the RF current at 13.56 MHz frequency mainly interacts with membrane rafts [14]. Therefore, the interaction of the RF-field with the BBB can improve BBB permeability, leading to increased therapeutic efficacy of drugs related to CNS diseases [16].

Furthermore, several studies have shown that an electromagnetic pulse could open the BBB locally, transiently, and reversibly [17]. A reversible opening strategy to enhance the permeability of drugs across the BBB can result in improved therapies due to enhanced drug bioavailability [18]. However, the role of the electromagnetic field in BBB permeability is still not fully understood [19]. Regardless of the precise mechanism of this interaction and considering that RF exposure mostly interacts with the cell membrane, we can try RF-field exposure to increase BBB permeability. To the best of our knowledge, there are no published reports that investigate BBB permeability at the medical band frequency (13.56 MHz) of the RF-field alone or in combination with SPIONs and *m*-PNPs. Therefore, the aim of this study was to investigate whether RF can enhance BBB permeability alone or in the presence of magnetic nanoparticles by using an *in vitro* BBB model.

2. Materials and methods

2.1. Materials

HTS Transwell (CLS3379, 24-well, 0.4 μm pore size, 6.5 mm inserts), fluorescein isothiocyanate (FITC) dextran (MW:4000), iron assay kit (MAK025), collagen from human placenta type IV (C5533), fibronectin from bovine plasma (F1141), potassium hexacyanoferrate (II) trihydrate, Hank's balance salt solution (HBSS, without phenol red, calcium chloride, magnesium), cyclohexane, polyvinylpyrrolidone (PVP), tertiary butanol, potassium carbonate (K_2CO_3), potassium permanganate ($KMnO_4$), and sodium periodate ($NaIO_4$) were purchased from Sigma-Aldrich, Germany. All other chemicals were obtained from Sigma-Aldrich unless specifically mentioned otherwise.

2.2. Fabrication of magnetic PLGA-b-PEG nanoparticles

Hydrophobic superparamagnetic iron oxide nanoparticles (SPIONs) were obtained by using the thermal decomposition method as reported in our previous studies [16,20]. Apart from our previous studies, the synthesized hydrophobic SPIONs were transferred to aqueous solution by a phase transfer process for biological applications in this study [21]. First, 100 mg of hydrophobic SPIONs were dispersed in 50 mL of cyclohexane. Then, 35 mL of tertiary butanol, 2.5 mL of K_2CO_3 (5%, w/w), 5 mL of a PVP aqueous solution (40%, w/w), and 20 mL of an oxidizing solution (9 mg $KMnO_4$ and 450 mg $NaIO_4$ aqueous solution) were added to that SPIONs solution. The obtained solution was then stirred at room temperature for 2 h. After that, the solution was washed and centrifuged with ethanol and water several times. Finally, the hydrophilic SPIONs were dispersed in water, filtered through a syringe filter (0.22 μm), and stored at 4 °C until use. Additionally, single emulsion solvent evaporation method was used to prepare magnetic PLGA-b-PEG nanoparticles (*m*-PNPs), which was reported in our previous study [16,22].

2.3. In vitro cell culture studies

Human umbilical vein endothelial cells (HUVECs) and human glioblastoma cells (T98G cell line) were used in cell culture studies. HUVECs were cultured in RPMI-1640 medium containing 10% (v/v) fetal bovine serum (FBS), 1% (v/v) penicillin-streptomycin and 1% (v/v) L-glutamine. T98G cells were cultured in Dulbecco's Modified Eagle's Medium F-12 (DMEM F-12) containing L-glutamine, supplemented with 10% (v/v) FBS and 1% (v/v) penicillin-streptomycin. All cultures and incubations were performed at 37 °C in a humidified atmosphere including 5% CO_2.

2.3.1. Coculture of HUVECs and T98G cells

To establish the *in vitro* blood-brain barrier model, the transwell membranes were coated with collagen type IV (10 μg/cm^2) and fibronectin (3 μg/cm^2) overnight before seeding the cells. HUVECs were seeded at a density of 5×10^4 cells/well on the apical (upper) side of the membrane. After 3 days, T98G cells were seeded at a density of 5×10^4 cells/well on the bottom (basolateral) side. Cells were cocultured for an extra 3 days, with changing medium every day, at 37 °C and 5% CO_2 in the incubator (Fig. 1).

2.3.2. Transendothelial electrical resistance (TEER) measurement

The integrity of the cell monolayer was evaluated by measuring the TEER using an endothelial voltohmmeter (Millicell ERS-2, Millipore, Germany). The TEER value of an empty transwell coated with collagen type IV and fibronectin was subtracted from each measurement. All of the experiments were performed in triplicate (biological replicates), and each measurement was also performed in technical triplicate. The TEER values of cells were measured daily until TEER values became stable, and then inserts were exposed to nanoparticles w/wo RF-fields (Fig. 1).

2.3.3. FITC-dextran permeability assay

In vitro BBB permeability was quantitatively investigated by a FITC-dextran assay [23]. FITC-dextran at different concentrations (0–10 μg/mL) in HBSS was measured by a fluorescent spectrophotometer (PerkinElmer, Multimode Plate Reader, Ensight, USA), and a calibration curve was generated at 490/528 nm excitation/emission wavelengths. All the inserts were transferred to a 24-well plate that contained 600 μL/well HBSS solution before adding FITC-dextran solution. Then, 100 μL/well FITC-dextran (10 μg/mL) was added to the apical side of the transwell inserts. Samples were taken from the basolateral chambers of RF-field treated (10 min, 13.56 MHz, 80 W) or untreated inserts at different incubation times (0, 1, 2 and 3 h). After each incubation time, three aliquots of 100 μl were taken from each well and separately transferred to each blank-well of a 96-well plate. The amount of FITC-dextran passing through the inserts with or without applied RF-fields was determined with a fluorescent plate reader (Fig. 1).

2.3.4. Passage of NPs through an in vitro BBB model under RF-field

The passage of NPs through an *in vitro* BBB model under the RF-field was investigated at different times (0, 1 and 2 h). SPIONs and *m*-PNPs were diluted with fresh medium to a final concentration of 200 μg/mL, and solutions were then added into the inserts. The inserts were exposed to RF-field (13.56 MHz, 80 W) for 10 min. The RF-field was generated using a homemade RF-field system, which was described by its stepwise technical implementation in our

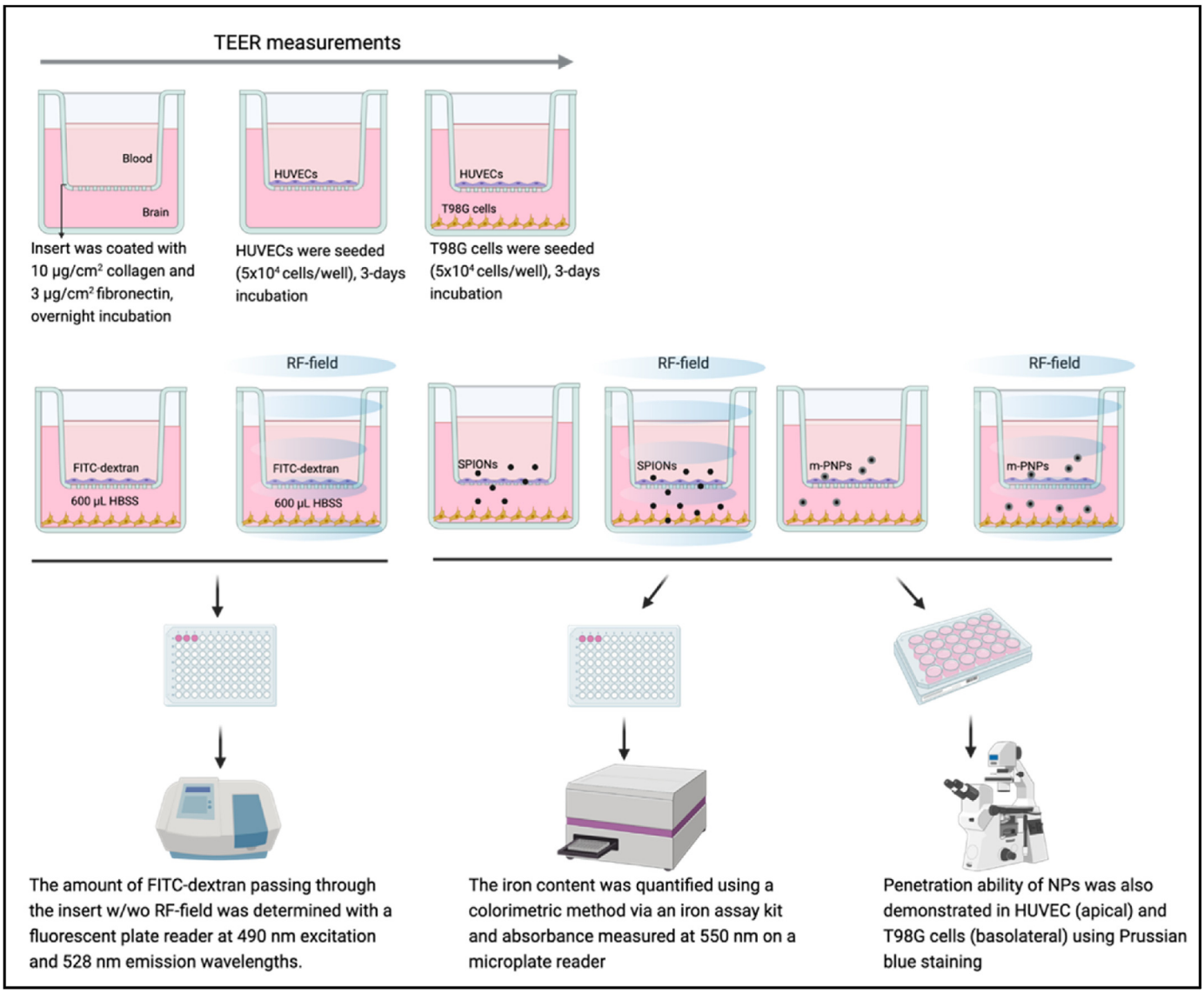


Fig. 1. Schematic representation of an *in vitro* BBB model, and the experimental design of the study (created with BioRender.com).

previous study [24].

2.3.5. Iron assay

The iron content in the nanoparticles was determined using an iron assay kit as described previously [16]. Briefly, after nanoparticles were treated in the presence or absence of an RF-field, the absorbance was measured at 593 nm with a microplate reader. Additionally, the iron concentration was calculated according to the calibration curve that was created with standard iron kit solutions (0–10 nmol/well) for 96-well plates.

2.3.6. Prussian blue staining

Intracellular ferric ions were investigated by Prussian blue staining [25]. Nanoparticles and RF-fields were applied to the inserts as detailed in Section 2.3.4. Subsequently, the culture medium was removed, and the cells on both sides (apical HUVECs and basolateral T98G cells) were gently washed three times with PBS and fixed with 4% paraformaldehyde for 15 min. Thereafter, the cells were stained with Prussian blue staining solution (2% hydrochloric acid and 2% potassium ferrocyanide (II) trihydrate) for 30 min at 37 °C. Finally, the cells were washed again three times with PBS, and the stained plate was observed using a light microscope (Olympus IX71, Japan).

2.4. Statistical analysis

The data was represented as the mean ± standard deviation (SD) of five replicates unless otherwise stated. Statistical analyses were performed by one-way analysis of variance (ANOVA) followed by Sidak's posttest with GraphPad Prism version 9 (GraphPad Software Inc., CA, USA), and p-values less than 0.05 were significant ($*p \leq 0.05$, $**p \leq 0.01$, $***p \leq 0.001$).

3. Results and discussion

3.1. Synthesis and characterization of m-PNPs

The transport capability of SPIONs across the BBB has many advantages, such as enhancing image contrast in magnetic resonance imaging (MRI), and the induction ability of SPIONs by

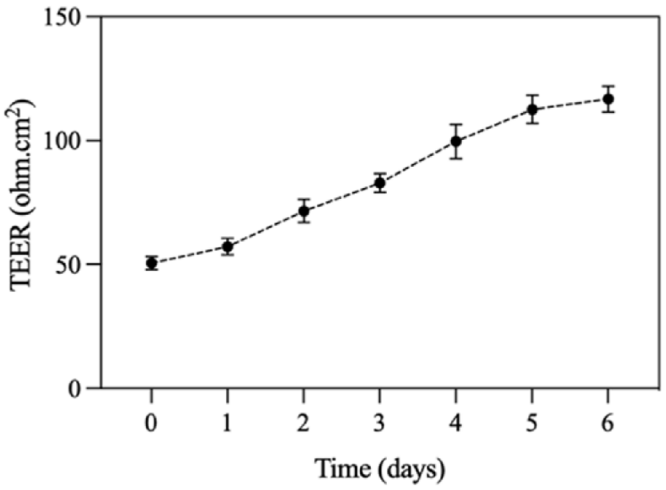


Fig. 2. TEER measurements of HUVECs (0–3 days) and HUVEC/T98G coculture (3–6 days).

hyperthermia for tumor therapy [26]. However, the application of SPIONs for imaging and therapeutic interventions in CNS disorders remains as a significant challenge [27]. Synthesis procedures and all characterization results of SPIONs, PLGA-b-PEG di-block copolymer, and magnetic PLGA-*b*-PEG NPs (*m*-PNPs) were reported in our previous publication [16]. Briefly, it was found that SPIONs (~5 nm) were highly monodisperse and uniform morphology. Furthermore, both SPIONs (core) and polymer (shell) exhibited well-defined spherical shapes with no particle aggregation [16].

3.2. Transendothelial electrical resistance (TEER) measurement

TEER was measured to assess the integrity or tightness of the *in vitro* BBB model. HUVECs were cultured as a monolayer on the apical side of inserts. After 3 days of incubation, T98G cells were seeded on the basolateral side, and HUVEC/T98G coculture was incubated for an extra 3 days. On day 6, the TEER value in the coculture was ~120 Ω cm^2 (Fig. 2). Shi et al. showed that endothelial/astrocyte cocultured cells have an ~120 Ω cm^2 TEER value after five days [28]. We found that the TEER value almost reached a plateau after 6 days, proposing an optimized culturing conditions for an *in vitro* BBB model.

3.3. FITC-dextran permeability assay

To evaluate the effects of RF on BBB permeability, the *in vitro* BBB model was exposed to an RF-field (10 min, 80 W, 13.56 MHz) in the presence of FITC-dextran solution. First, the fluorescence intensity of FITC-dextran at different concentrations (0–10 μg/mL) in HBSS solution was used to obtain a standard calibration curve (Fig. 3a). Then, the fluorescence intensities were measured by taking the solutions from the lower chamber at 0, 1, 2, and 3 h (Fig. 3b). Immediately after the RF-field exposure (0 h), the amount of FITC-dextran was found to be almost 10-fold higher than that of the RF (−) group (***$p \leq 0.001$). This result suggested that RF acts as the initial burst phase through the BBB model, like the drug release profiles of some nanoparticles. In other words, a low level of FITC-dextran was observed in the lower chamber following the application of FITC-dextran alone (RF (−)) at 0 h. However, in the RF (−) group, the FITC-dextran passing to the basolateral side reached the same level as the RF (+) group at the end of the 1st h. On the other hand, significant increases were observed again in the RF (+) group

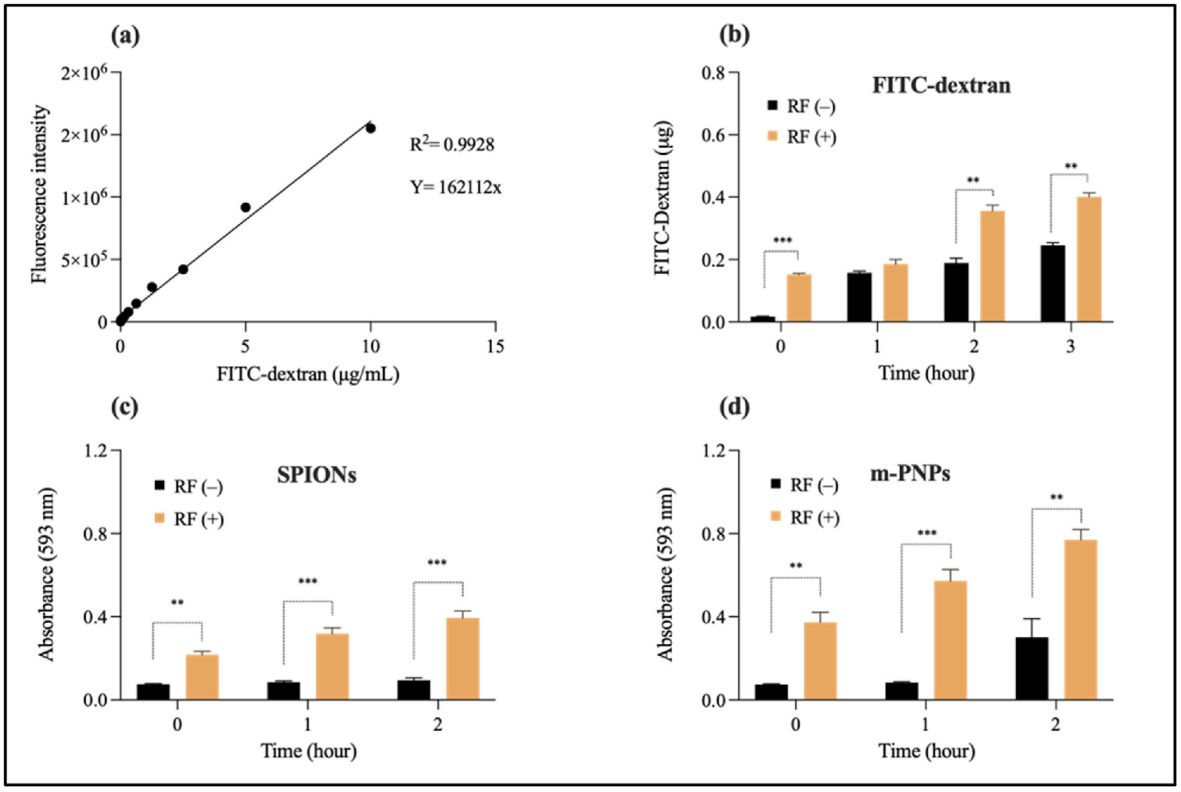


Fig. 3. (a) FITC-dextran fluorescence intensity–concentration curve (0–10 μg/mL). (b) The amount of FITC-dextran in the basolateral chambers with or without RF-field (time scale bar represents just after 10 min RF-field exposure). The amount of iron in the basolateral chambers with or without RF-field treated with (c) SPIONs or (d) *m*-PNPs.

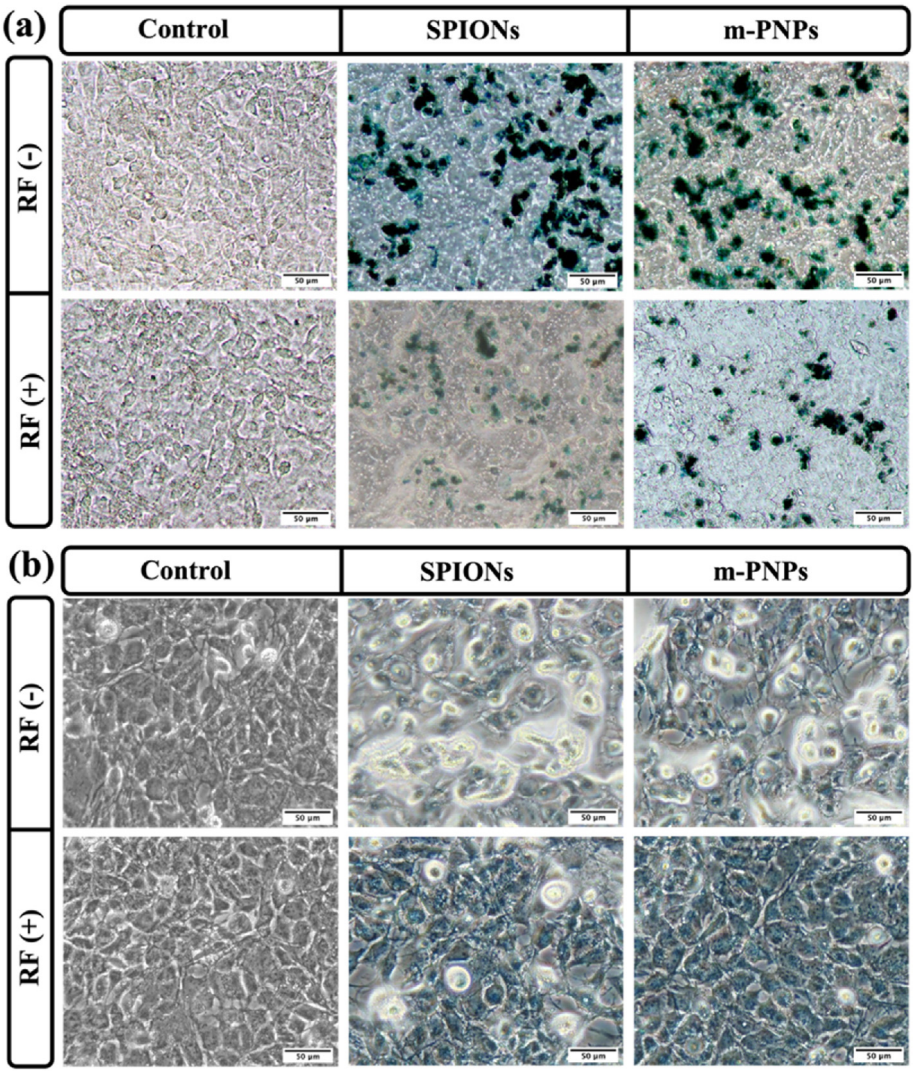


Fig. 4. Prussian blue staining images of (a) HUVECs (apical side) and (b) T98G cells (basolateral side) with SPIONs and *m*-PNPs in the presence and absence of RF-field. (For interpretation of the references to colour in this figure legend, the reader is referred to the Web version of this article.)

according to RF (−) at the 2nd and 3rd h. Therefore, the RF effect may have acted as an initial burst followed by a slower phase for BBB permeability. This phenomenon, which can be called as the burst-permeability RF effect (BP-RF), is presented here for the first time in the literature. The RF current with a frequency of 13.56 MHz cannot penetrate into the cell interior as the cell membrane is an excellent electrical insulator. Additionally, RF-fields mostly interact with cell membrane dynamic structures, which compose of tightly packed microdomains (lipid rafts) [29]. Therefore, it seems possible that the RF-field can increase the FITC-dextran permeability by interacting directly with the dynamic structures of the cell membranes.

3.4. Passage of NPs through an in vitro BBB model under RF-field

The effect of the RF-field on the permeability of the *in vitro* BBB model in the presence of nanoparticles was determined by calculating the amount of total iron in the receiving chambers. Additionally, to test the final iron oxide concentration, solutions in the receiving chambers were collected, and the concentration was measured using an iron assay kit. In the RF (−) group, NPs transport from the apical to the basolateral side was limited for both SPIONs and *m*-PNPs. In fact, the amount of SPIONs on the basolateral side did not increase over time (Fig. 3c), which may be related to the aggregation of SPIONs, even if phase transfer was performed. However, the amount of *m*-PNPs in the receiving chamber increased at 2 h in the RF (−) group (Fig. 3d). This situation can be interpreted as PLGA-b-PEG polymers partially facilitating the transition from the *in vitro* BBB, and *m*-PNPs have lower aggregate tendencies than the SPIONs. However, the amount of SPIONs and *m*-PNP transferred to the basolateral side at 0, 1 and 2 h after RF-field exposure increased as statistically significant for both NPs compared to the RF (−) group (Fig. 3c and d). In addition to this, over time, the amount of both transported NPs increased on the basolateral sides in the presence of an RF-field. In the light of our results, we can conclude that RF-field exposure increased the BBB permeability of SPIONs and *m*-PNPs in our *in vitro* BBB model.

The effect of RF-field at 13.56 MHz frequency was approved in the cell membrane bilayer, and the RF-field can alter the ionic gradient across the membrane [15]. Wust et al. showed that RF creates nonthermal effects that occur at the cell membrane by altering ion transitions [14]. Moreover, membrane microdomains, also called lipid rafts, have dynamic structures that may play a crucial role in the interaction of the membrane with the RF-field

[30,31]. Zhou et al. studied the effect of electromagnetic pulses (EMPs) on the permeability of an *in vitro* BBB model. They found that EMP exposure increased the BBB permeability at 1–12 h and that the permeability returned to its normal level at 24 h [32]. Do et al. showed that the exposure of external electromagnetic fields with magnetic nanoparticles facilitated the permeability of the BBB in a mouse model [33]. In our study, RF-BBB interactions in the presence of SPIONs and *m*-PNPs increased the permeability of the *in vitro* BBB model. Therefore, the RF-field can enhance BBB permeability, which leads to enhanced efficiency of the therapeutic agents.

3.5. Prussian blue staining

To further investigate the relationship between the RF-field and penetration of SPIONs and *m*-PNPs, HUVECs (apical) and T98G cells (basolateral) were also stained by Prussian blue (Fig. 4). Prussian blue staining is a common method used to detect iron in tissue or cells [34]. In the absence of an RF-field in HUVECs (Fig. 4a), SPIONs and *m*-PNPs were stained intensely blue, indicating that NPs were more deposited on the apical side of the transwell membrane. In other words, magnetic nanoparticles were accumulated (or aggregated) in the membranes of the RF (−) groups, and Prussian blue staining was strongly positive in HUVECs. However, after the RF-field was applied, the intensity of Prussian blue staining decreased compared to that in the RF (−) group (Fig. 4a). Dan et al. showed that alternating magnetic fields increased the uptake of SPIONs in murine brain endothelial cell lines [35]. On the other hand, NPs penetrating from the membrane to the basolateral side (T98G cells) by the RF-effect were stained intensely as dark blue compared to the RF (−) group (Fig. 4b). Additionally, NPs that accumulate in T98G cells by crossing the membrane under an RF-field can be seen as blue areas or spots in almost every cell. Moreover, Prussian blue staining indicated the transport of magnetic NPs across the BBB because of the effective interaction between RF and the *in vitro* BBB model. The Prussian blue staining was also consistent with our iron assay kit results.

4. Conclusion

In this study, an *in vitro* BBB model was successfully established based on TEER measurements of HUVEC/T98G cocultured cells. This model was then used to evaluate BBB permeability under an RF-field alone or in combination with the nanoparticles (SPIONs, *m*-PNPs). Notably, the interaction of the RF-field alone and the *in vitro* BBB model increased FITC-dextran permeability by 10-fold immediately after RF was applied. We defined this phenomenon as the burst-permeability RF effect (BP-RF). The BP-RF effect can increase the treatment efficacy of CNS diseases by enabling higher drug transit through the BBB. In addition to this, Fe quantification levels in the lower chamber reveals that the RF combination with membrane or nanoparticles (SPIONs, *m*-PNPs) also enhanced the *in vitro* BBB permeability. Overall, RF may be an alternative route that can transiently stimulate the BBB to increase the access of drugs to the brain.

Declaration of interests

☒ The authors declare that they have no known competing financial interests or personal relationships that could have appeared to influence the work reported in this paper.

☐The authors declare the following financial interests/personal relationships which may be considered as potential competing interests:

Declaration of competing interest

There is no conflict of interest.

Acknowledgement

This study was supported by the Scientific and Technological Research Council of Turkey (TUBITAK), Grant no: SBAG-119S137. We are sincerely grateful for the assistance of the Cell and Tissue Engineering Research Group at Hacettepe University, and Dr. Anıl Sera Cakmak for the cell culture studies. We are also thankful to Dr. Guldeniz Selmanoglu, Dr. Elif Karacaoglu and Deniz Tulumcuoglu for their support in TEER measurements. We are sincerely grateful to Dr. Cagatay Karaaslan and Dilara Karaguzel for their assistance in fluorescence plate reader measurements.

References

[1] S.F. Spampinato, S. Merlo, E. Fagone, M. Fruciano, C. Barbagallo, T. Kanda, Y. Sano, M. Purrello, C. Vancheri, M. Ragusa, Astrocytes modify migration of PBMCs induced by β-amyloid in a blood-brain barrier in vitro model, Front. Cell. Neurosci. 13 (2019) 337.
[2] Q. Lu, X. Cai, X. Zhang, S. Li, Y. Song, D. Du, P. Dutta, Y. Lin, Synthetic polymer nanoparticles functionalized with different ligands for receptor-mediated transcytosis across blood-brain barrier, ACS Appl Bio Mater 1 (5) (2018) 1687–1694.
[3] D. Upreti, D. Bakhshinyan, D. Bloemberg, P. Vora, C. Venugopal, S.K. Singh, Strategies to enhance the efficacy of T-cell therapy for central nervous system tumors, Front. Immunol. 11 (2020).
[4] W. Löscher, A. Friedman, Structural, molecular, and functional alterations of the blood-brain barrier during epileptogenesis and epilepsy: a cause, consequence, or both? Int. J. Mol. Sci. 21 (2) (2020) 591.
[5] X. Dong, Current strategies for brain drug delivery, Theranostics 8 (6) (2018) 1481–1493.
[6] S. Sahab-Negah, F. Ariakia, M. Jalili-Nik, A.R. Afshari, S. Salehi, F. Samini, G. Rajabzadeh, A. Gorji, Curcumin loaded in niosomal nanoparticles improved the anti-tumor effects of free curcumin on glioblastoma stem-like cells: an in vitro study, Mol. Neurobiol. 57 (2020) 3391–3411.
[7] W. Ran, X. Xue, Theranostical application of nanomedicine for treating central nervous system disorders, Sci. China Life Sci. 61 (4) (2018) 392–399.
[8] T. Sun, A. Dasgupta, Z. Zhao, M. Nurunnabi, S. Mitragotri, Physical triggering strategies for drug delivery, Adv. Drug Deliv. Rev. 158 (2020) 36–62.
[9] F. Senturk, S. Çakmak, G.G. Ozturk, Synthesis and characterization of oleic acid coated magnetic nanoparticles for hyperthermia applications, Natural and Applied Sciences Journal 2 (2) (2019) 16–29.
[10] Q. He, J. Liu, J. Liang, X. Liu, W. Li, Z. Liu, Z. Ding, D. Tuo, Towards improvements for penetrating the blood–brain barrier—recent progress from a material and pharmaceutical perspective, Cells 7 (4) (2018) 24.
[11] B.S. Mahmoud, A.H. AlAmri, C. McConville, Polymeric nanoparticles for the treatment of malignant gliomas, Cancers 12 (1) (2020) 175.
[12] B. Sırav, N. Seyhan, Effects of GSM modulated radio-frequency electromagnetic radiation on permeability of blood–brain barrier in male & female rats, J. Chem. Neuroanat. 75 (2016) 123–127.
[13] L. Huerta-Nuñez, G. Gutierrez-Iglesias, A. Martinez-Cuazitl, M. Mata-Miranda, V. Alvarez-Jiménez, V. Sánchez-Monroy, A. Golberg, C. González-Díaz, A biosensor capable of identifying low quantities of breast cancer cells by electrical impedance spectroscopy, Sci. Rep. 9 (1) (2019) 1–12.
[14] P. Wust, B. Kortüm, U. Strauss, J. Nadobny, S. Zschaeck, M. Beck, U. Stein, P. Ghadjar, Non-thermal effects of radiofrequency electromagnetic fields, Sci. Rep. 10 (1) (2020) 1–8.
[15] G. Andocs, M. Rehman, Q. Zhao, Y. Tabuchi, M. Kanamori, T. Kondo, Comparison of biological effects of modulated electro-hyperthermia and conventional heat treatment in human lymphoma U937 cells, Cell death discovery 2 (1) (2016) 1–10.
[16] F. Senturk, S. Cakmak, I.C. Kocum, M. Gumusderelioglu, G.G. Ozturk, GRGDS-conjugated and curcumin-loaded magnetic polymeric nanoparticles for the hyperthermia treatment of glioblastoma cells, Colloids Surf. A Physicochem. Eng. Asp. (2021) 126648.
[17] H. Nittby, A. Brun, J. Eberhardt, L. Malmgren, B.R. Persson, L.G. Salford, Increased blood–brain barrier permeability in mammalian brain 7 days after exposure to the radiation from a GSM-900 mobile phone, Pathophysiology 16 (2–3) (2009) 103–112.
[18] M. Kaiser, M. Burek, S. Britz, F. Lankamp, S. Ketelhut, B. Kemper, C. Förster, C. Gorzelanny, F.M. Goycoolea, The influence of capsaicin on the integrity of microvascular endothelial cell monolayers, Int. J. Mol. Sci. 20 (1) (2019) 122.
[19] S. Wang, Z. Song, H. Li, G. Guo, X. Xi, Numerical simulation and analysis of effects of individual differences on the field distribution in the human brain with electromagnetic pulses, Sci. Rep. 11 (1) (2021) 1–8.
[20] F. Senturk, S. Cakmak, M. Gumusderelioglu, G.G. Ozturk, Hydrolytic instability

and low-loading levels of temozolomide to magnetic PLGA nanoparticles remain challenging against glioblastoma therapy, J. Drug Deliv. Sci. Technol. (2022) 103101.
[21] J. Cai, Y.Q. Miao, B.Z. Yu, P. Ma, L. Li, H.M. Fan, Large-scale, facile transfer of oleic acid-stabilized iron oxide nanoparticles to the aqueous phase for biological applications, Langmuir 33 (7) (2017) 1662–1669.
[22] S.H. Chun, S.W. Shin, L. Amornkitbamrung, S.Y. Ahn, J.S. Yuk, S.J. Sim, D. Luo, S.H. Um, Polymeric nanocomplex encapsulating iron oxide nanoparticles in constant size for controllable magnetic field reactivity, Langmuir 34 (43) (2018) 12827–12833.
[23] D. Hoff, L. Sheikh, S. Bhattacharya, S. Nayar, T.J. Webster, Comparison study of ferrofluid and powder iron oxide nanoparticle permeability across the blood–brain barrier, Int. J. Nanomed. 8 (2013) 703.
[24] F. Senturk, I.C. Kocum, G. Guler Ozturk, Stepwise Implementation of a Low-Cost and Portable Radiofrequency Hyperthermia System for in Vitro/in Vivo Cancer Studies, Instrumentation Science & Technology, 2021, pp. 1–13.
[25] Y. Ling, K. Wei, Y. Luo, X. Gao, S. Zhong, Dual docetaxel/superparamagnetic iron oxide loaded nanoparticles for both targeting magnetic resonance imaging and cancer therapy, Biomaterials 32 (29) (2011) 7139–7150.
[26] Y. Huang, B. Zhang, S. Xie, B. Yang, Q. Xu, J. Tan, Superparamagnetic Iron oxide nanoparticles modified with tween 80 pass through the intact blood–brain barrier in rats under magnetic field, ACS Appl. Mater. Interfaces 8 (18) (2016) 11336–11341.
[27] Z. Sun, M. Worden, Y. Wroczynskyj, V. Yathindranath, J. van Lierop, T. Hegmann, D.W. Miller, Magnetic field enhanced convective diffusion of iron oxide nanoparticles in an osmotically disrupted cell culture model of the blood–brain barrier, Int. J. Nanomed. 9 (2014) 3013.
[28] G.M. Di Shi, S. Bhattacharya, S. Nayar, T.J. Webster, Optimizing superparamagnetic iron oxide nanoparticles as drug carriers using an in vitro blood–brain barrier model, Int. J. Nanomed. 11 (2016) 5371.
[29] A. Szasz, Thermal and nonthermal effects of radiofrequency on living state and applications as an adjuvant with radiation therapy, Journal of Radiation and Cancer Research 10 (1) (2019) 1.
[30] K. Hanafusa, T. Hotta, K. Iwabuchi, Glycolipids: linchpins in the organization and function of membrane microdomains, Front. Cell Dev. Biol. 8 (2020).
[31] A. Szasz, A bioelectromagnetic proposal approaching the complex challenges of COVID-19, Open J. Biophys. 11 (1) (2020) 1–67.
[32] J.X. Zhou, G.R. Ding, J. Zhang, Y.C. Zhou, Y.J. Zhang, G.Z. Guo, Detrimental effect of electromagnetic pulse exposure on permeability of in vitro blood-brain-barrier model, Biomed. Environ. Sci. 26 (2) (2013) 128–137.
[33] T.D. Do, F.U. Amin, Y. Noh, M.O. Kim, J. Yoon, Guidance of magnetic nanocontainers for treating Alzheimer's disease using an electromagnetic, targeted drug-delivery actuator, J. Biomed. Nanotechnol. 12 (3) (2016) 569–574.
[34] R. Afzalipour, S. Khoei, S. Khoee, S. Shirvalilou, N. Jamali Raoufi, M. Motevalian, M.R. Karimi, Dual-targeting temozolomide loaded in folate-conjugated magnetic triblock copolymer nanoparticles to improve the therapeutic efficiency of rat brain gliomas, ACS Biomater. Sci. Eng. 5 (11) (2019) 6000–6011.
[35] M. Dan, Y. Bae, T.A. Pittman, R.A. Yokel, Alternating magnetic field-induced hyperthermia increases iron oxide nanoparticle cell association/uptake and flux in blood–brain barrier models, Pharm. Res. (N. Y.) 32 (5) (2015) 1615–1625.